Relaxation Dynamics of Polymer Liquids in Nonlinear Step Shear

Lynden A. Archer,* Javier Sanchez-Reyes, and Juliani

School of Chemical Engineering, Cornell University, Ithaca, New York 1485

Received August 8, 2002; Revised Manuscript Received October 23, 2002

ABSTRACT: Relaxation dynamics of entangled polymer liquids are investigated in nonlinear step shear flow using mechanical rheometry experiments and theory. Entangled solutions of high molar mass polystyrenes (PS), $3 \times 10^5 \leq \phi\bar{M}_w \leq 1.6 \times 10^6$ g/mol, in diethyl phthalate (DEP) are the main focus of this study. Cone-and-plate rheometer fixtures roughened by attachment of a single layer of 10−30 μm silica glass beads are used to eliminate interfacial slip during step shear measurements. A simple theory for stress relaxation dynamics that accounts for coupled relaxation of molecular orientation, chain stretching, and entanglement density is used to analyze the experimental results. In PS/DEP solutions with $\phi\bar{M}_w \geq 5 \times 10^5$ and in which PS forms an average of eight or more entanglements per chain, we find that the nonlinear relaxation modulus can be factorized into separate strain-dependent and time-dependent functions only after a time $\lambda_{k2} \approx \tau_{d0} \sim (\phi\bar{M}_w)^3$ substantially larger than the longest Rouse relaxation time τ_{Rouse} of the solution. This finding is consistent with results from a previous study of step shear dynamics in solutions of ultrahigh molecular weight polystyrene, $\bar{M}_w = 2.06 \times 10^7$ [Sanchez-Reyes, J.; Archer, L. A. *Macromolecules* **2002**, *35*, 5194], but contradicts expectations from current theories for entangled polymer dynamics, which predict $\lambda_{k2} \approx (3 - 5)\tau_{Rouse}$. The origin of this discrepancy is traced to a greater than expected influence of entanglement loss and recovery processes on polymer relaxation dynamics in nonlinear step shear flow.

1. Introduction

Shear fields can cause polymer molecules in entangled solutions to orient, stretch, and disentangle from their neighbors. After the field is removed, thermal and elastic forces cause molecules to relax to recover their equilibrium orientation, length, and entanglement structure. The time scale on which each of these relaxation processes occurs need not be the same. Relaxation of macroscopic properties such as shear stress will, therefore, generally involve complex superposition of many molecular-scale dynamic processes. To develop quantitative molecular theories for stress relaxation in entangled polymer liquids, each of these processes must be understood and their contributions to the stress determined. Pioneering works by deGennes[1] and by Doi and Edwards,[2] for example, have resolved the processes by which entangled molecules relax orientation following cessation of shear. Theories for polymer contour length relaxation dynamics[2−4] and for field-induced changes in polymer entanglement structure[4] are not as well developed.

Step shear experiments provide a valuable tool for investigating stress relaxation dynamics in polymers. In a step shear deformation, a material is subjected to time-dependent shear strain $\gamma(t) = \gamma H(t)$. The resulting time-dependent shear stress $\sigma(t,\gamma)$ developed in the material is measured and used to determine its nonlinear shear relaxation modulus $G(t,\gamma) = \sigma(t,\gamma)/\gamma$. In most practical situations $H(t)$ is not a true Heaviside function, but approaches one on time scales of order 10−100 ms after commencing the step. $G(t,\gamma)$ therefore provides information about all but the fastest relaxation processes in the material and about how these processes are affected by strain amplitude γ. In nearly monodisperse entangled linear polymers, two relaxation processes predominate−a fast process (thought to arise from relaxation of molecular stretching) and a slow process (reflecting relaxation of molecular orientation).[2,5] Faster processes associated with equilibration of the surrounding polymer network structure and of uneven deformation along polymer chains are believed to occur on time scales that are beyond the reach of most step shear experiments. In many molecular theories the fast chain stretch relaxation and slow molecular reorientation processes are assumed to be completely decoupled; however, some theories do anticipate coupling of these processes.[4]

Step shear experiments on entangled polymer solutions have long been recognized as important for resolving the molecular mechanisms for polymer length relaxation.[2,5−8] These experiments are limited, however, by the possibility of significant levels of interfacial slip.[9] The most plausible mechanisms for interfacial slip in polymers suggest that slip is itself time-dependent and that the magnitude of interfacial slip is generally a nonlinear function of shear stress. Thus, wall slip errors affect the magnitude and time dependence of $G(t,\gamma)$ in very different ways, preventing simple slip correction procedures after the fact (e.g., step shear measurements using parallel plate fixtures with variable gaps can be used to quantify then correct slip errors). Recently, Sanchez-Reyes and Archer proposed a simple method for reducing errors due to wall slip in step shear deformations.[10] In this procedure, a single layer of micro- or nanosized silica spheres is grafted to cone-and-plate mechanical fixtures used to generate shear. Using this procedure, the authors investigated relaxation dynamics of entangled solutions of an ultrahigh molar mass polystyrene ($\bar{M}_w = 20.06 \times 10^6$ g/mol, $\bar{M}_n = 1.672 \times 10^6$ g/mol, PS20M) in diethyl phthalate (DEP).[10] The entanglement density $N/N_e(\phi)$ of PS20M was varied from 4 to 37 by changing the polymer volume fraction ϕ in solution. Step shear measurements for the high and intermediate solution concentrations were performed using cone-and-plate fixtures with a variety of cone angles $1° \leq \alpha \leq 5°$ to evaluate the effect of interfacial slip on material response. The authors reported two dominant relaxation processes in these systems. The

10.1021/ma021286q CCC: $22.00
Published on Web 11/27/2002

Table 1. Physical Properties of PS/DEP Solutions Used in This Study

solution	$\bar{M}_w \times 10^6$	PI	ϕ	G_N (Pa)	τ_e (s)	τ_{Rouse} (s)	η_0 (Pa·s)	τ_{d0} (s)
PS3.8M8%	3.84	1.04	0.077	550	3.2×10^{-4}	0.18	6.9×10^{-2}	2.9
PS5.4M6%	5.48	1.15	0.058	297	4.8×10^{-4}	0.19	5.1×10^{-2}	7.3
PS8.4M6%	8.42	1.2	0.067	375	3.6×10^{-4}	0.49	2.4×10^{-3}	24.1
PS20M6%	20.1	1.2	0.064	340	4.1×10^{-4}	0.92	2.9×10^{-4}	363.2

first, fast relaxation process was characterized by a time constant $\lambda_{k1} = (16.5 \pm 4.7)\tau_{Rouse}$, which increased with solution concentration as $\lambda_{k1} \sim \phi^{0.7}$. The time constant for the second process $\lambda_{k2} \propto \tau_{d0}$ also increased with solution concentration $\lambda_{k2} \sim \phi^{3.2}$.

Significantly, Sanchez-Reyes and Archer found that while the fast relaxation process is dominated by relaxation of polymer chain stretching, the second process includes both stretch and orientation relaxation contributions. The authors also found that while the apparent shear damping function $h(\gamma,t) \equiv G(t,\gamma)/G(\gamma\rightarrow 0,t)$ approaches the universal damping function $h_{DE-IA}(\gamma)$ predicted by the Doi−Edwards theory[2] on time scales of order λ_{k1}, the nonlinear relaxation modulus $G(t,\gamma)$ could only be factorized into separate time-dependent $G(t)$ and strain-dependent $h(\gamma)$ functions after a time of order λ_{k2}, which is generally larger than λ_{k1}. On time scales intermediate between λ_{k1} and λ_{k2}, $G(t,\gamma)h^{-1}(\gamma)$ manifests complicated strain-dependent behavior and $h(\gamma,t)$ displays a small, but well-defined, local minimum.[10] A more in-depth study, focusing particularly on of the latter two results, should shed light on the molecular processes that couple chain stretching and orientation relaxation processes in entangled polymer liquids.

2. Experiment

2.1. Materials. Several narrow molecular weigh distribution, high molar mass polystyrenes $20.06 \times 10^6 \leq \bar{M}_w \leq 1.8 \times 10^6$ g/mol were purchased from Tosoh Corp., Japan, and Aldrich. Entangled solutions of each polymer in diethyl phthalate (DEP, [Aldrich]) were formulated using dichloromethane (methylene chloride, [Aldrich]) as cosolvent. Solutions required extremely long periods for solvent evaporation, 3−4 months at room temperature, to completely remove all traces of the cosolvent without introducing concentration inhomogeneties and air bubbles. The volume fraction of polymer and the respective entanglement densities $N/N_e = \bar{M}_w\phi^{1.3}/M_{eo}$ for each solution is provided in Table 1. Here $M_{eo} \approx 18\,000$ g/mol is the molar mass of polystyrene segments between entanglement points.

2.2. Viscoelastic Characterization. Linear viscoelastic properties of all PS/DEP solutions were characterized by small-amplitude oscillatory shear measurements using a Paar Physica modular compact (MCR 300) rheometer over a wide temperature range, $-40\ °C \leq T \leq 28.5\ °C$. Measurements were performed using 50, 15, and 6 mm diameter parallel plate fixtures, and temperature regulation was achieved using liquid nitrogen. To simultaneously maximize signal-to-noise and minimize measurement errors due to frame and transducer compliance, the largest plate diameters were used to measure storage $G'(\omega)$ and loss moduli $G''(\omega)$ at high temperatures and low frequencies, and the smallest fixtures were used for low-temperature and high-frequency experiments. Time−temperature superposition was used to generate master curves at 28.5 °C spanning nearly 13 decades of frequency. Results for two materials PS8.4M6% and PS3.8M8% are provided in Figures 1a and 2a, respectively.

Terminal viscoelastic properties were obtained from the master curves using the following standard relations, $\eta_0 = \lim_{\omega\rightarrow 0}(G''(\omega)/\omega)$ and $\tau_{d0} = J_e^0\eta_0$,[11] and the plateau modulus G_N was estimated as the storage modulus value at the loss minimum in the rubbery plateau regime. Results for all polymers studied are provided in Table 1. Figures 1b and 2b

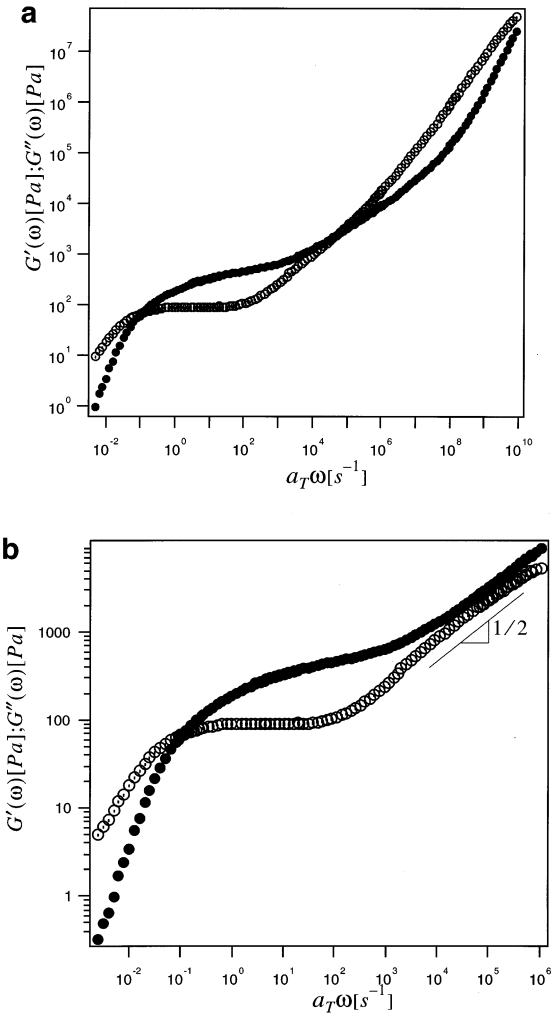

Figure 1. (a) Dynamic storage $G'(\omega)$ (filled symbols) and loss moduli $G''(\omega)$ for PS8.4M6%. Measurements were performed over a broad range of temperature, $-40\ °C \leq T \leq 28.5\ °C$, and the results shifted to 28.5 °C using time−temperature superposition. (b) Dynamic storage $G'(\omega)$ (filled symbols) and loss moduli $G''(\omega)$ for PS8.4M6% at 28.5 °C with the high-frequency solvent and segmental contributions removed. The frequency scalings now apparent at high frequency, $G'(\omega) \sim G''(\omega) \sim \omega^{1/2}$, are consistent with Rouse dynamics of polymer molecules in solution.

were obtained by subtracting multimode Maxwell model fits of the high-frequency data in Figures 1a and 2a from the respective storage and loss moduli data. This procedure removes segmental and solvent contributions from the measured storage and loss moduli. The success of the approach can be easily appreciated from the nearly exact Rouse frequency scalings of $G'(\omega)$ and $G''(\omega)$ in the dynamic regime preceding the onset of the rubbery plateau. Entanglement Rouse relaxation times τ_e were obtained from the intersection of the Rouse regime and the rubbery plateau for each solution. Longest Rouse relaxation times τ_{Rouse} were determined by fitting the high-frequency storage moduli (Figures 1b and 2b) with the Rouse result for polystyrene solutions $G'(\omega) = (1.11cRT/M)(\tau\omega)^{1/2}$.[12] τ_{Rouse} values obtained using this approach are provided in Table 1. Values of the Rouse relaxation time τ_R calculated from η_0 using the method of Menezes and

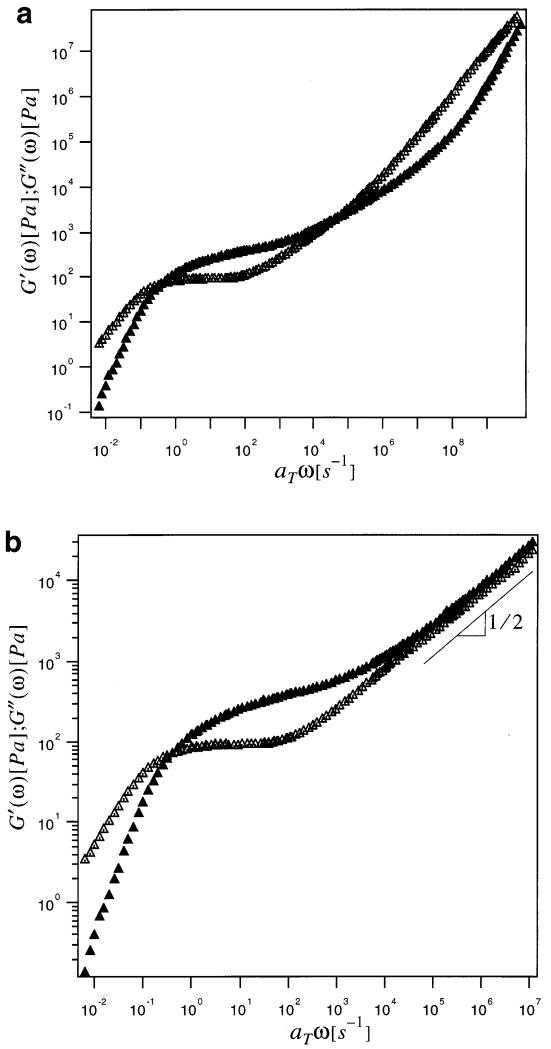

Figure 2. (a) Dynamic storage $G'(\omega)$ (filled symbols) and loss moduli $G''(\omega)$ for PS3.8M8%. Measurements were performed over a broad range of temperature, $-40\ °C \le T \le 28.5\ °C$, and the results shifted to 28.5 °C using time−temperature superposition. (b) Same as (a) but with the high-frequency solvent and segmental contributions removed. Again, at high frequencies storage and loss moduli display nearly perfect Rouse frequency scalings $G'(\omega) \sim G''(\omega) \sim \omega^{1/2}$.

Table 2. Experimental and Theoretical Separability Times for PS/DEP Solutions

solution	λ_{k1}(s)	λ_{k2} (s)	$\lambda_{k1;T}$ (s)	$\lambda_{k2;T}$ (s)	τ_R (s)
PS3.8M8%	1.2	1.3	0.9	2.9	0.23
PS5.4M6%	1.6	2.1	1.0	4.6	0.22
PS8.4M6%	4.9	33.4	2.2	22.5	0.44
PS20M6%	12	281.4	6.9	400	1.06

Graessley[13] are provided in Table 2. Considering the uncertainties in the data required to calculate τ_{Rouse} by either method, the agreement between τ_{Rouse} and τ_R values may be considered very good for all materials used in the study. This conclusion disagrees with findings reported in ref 14, where significant differences in τ_{Rouse} were found using the two procedures. We suspect that the small magnitudes and narrow range of τ_{Rouse} values of the systems studied here may obscure differences in τ_{Rouse} values obtained using the two methods.

Step shear measurements were performed at 28.5 °C using the MCR equipped with 50 mm diameter cone-and-plate fixtures. As in the earlier work,[10] a single layer of 10−30 μm silica glass beads was attached to each fixture to minimize interfacial slip. Step shear measurements were also repeated at multiple cone angles, 1°, 2°, 3°, and 5°, to independently evaluate the effectiveness of the bead-grafting technique for reducing slip. Other details of the step shear measurements are the same as reported in ref 10.

3. Results and Discussion

3.1. Experiment. Nonlinear shear relaxation moduli ($G(t,\gamma) \equiv \sigma(t,\gamma)/\gamma$ for PS8.4M6%, $N/N_e(\phi) = 13$) are provided in Figure 3a. These measurements were performed using 1°, 50 mm diameter cone-and-plate fixtures grafted with silica beads. The experimental results are presented at several shear strains. At times $t > 10$ s, $G(t,\gamma)$ curves are visibly parallel to each other for all shear strains studied. This feature of the results is a well-known signature of the fact that $G(t > 10\ s, \gamma)$ can be factorized into separate time-dependent $G(t)$ and strain-dependent $h(\gamma)$ functions. Figure 3b depicts the shifted nonlinear relaxation modulus $G(t,\gamma)\ h(\gamma)^{-1}$ for PS8.4M6% over the same range of shear strain. These results show that the long-time $G(t,\gamma)$ curves at variable shear strain γ are never exactly parallel but that at times beyond a characteristic separability time, $\lambda_{k2} \approx 33$ s, $G(t,\gamma)$ is approximately parallel at all strains. This indicates that time strain factorability is only approximate in this material—a trait that is shared with most entangled solutions of high molar mass polystyrenes in diethyl phthalate.[8,10]

The separability time λ_{k2} for PS8.4M6% is evidently almost 50 times its longest Rouse relaxation time. λ_{k2} is however of similar magnitude to the terminal relaxation time τ_{d0} of this solution, $\lambda_{k2} \approx 1.4\tau_{d0}$. Both features of the separability time of PS8.4M6% are shared by the more highly entangled PS20M6% ($N/N_e(\phi) = 31$, $\lambda_{k2} \approx 0.78\tau_{d0} \approx 300\tau_{Rouse}$) solution and somewhat less by PS5.4M6% ($N/N_e(\phi) = 8$, $\lambda_{k2} \approx 0.29\tau_{d0} \approx 11\tau_{Rouse}$). The corresponding $G(t,\gamma)\ h(\gamma)^{-1}$ data for the least entangled polymer solution, PS3.8M8% ($N/N_e(\phi) = 6$), are presented in Figure 4. In this case, $G(t,\gamma)$ is seen to be factorable over a much broader time range. The separability time $\lambda_{k2} \approx 1.3$ s is still substantially larger than the longest Rouse relaxation time, $\lambda_{k2} \approx 7.2\tau_{Rouse} \approx 0.44\tau_{d0}$, but the relationship between the two time scales is in better agreement with recent data from the literature.[10,14,15] Thus, although the experimental results do show an overall stronger alignment of the separability time with the terminal time τ_{d0}, the separability time approaches τ_{Rouse} as the entanglement density of PS/DEP solutions is lowered. This feature of the data is consistent with earlier observations for PS20M/DEP solutions.[10]

As discussed in the previous study, factorability can also be determined from the apparent damping function $h(\gamma,t) \equiv G(t,\gamma)/G(\gamma \to 0, t)$. In this case the time required for $h(\gamma,t)$ to achieve its long-time value is the separability time. Figure 5a,b summarizes $h(\gamma,t)$ for two of the polymers studied. For the more highly entangled material, PS8.4M6%, $h(\gamma,t)$ approaches what appears to be its final value in a time $\lambda_{k1} \approx 3.5$ s but then goes through a shallow local minimum at longer times and never fully achieves a constant value. The minimum is in fact sufficiently shallow that on a coarse linear scale $h(\gamma,t)$ appears to reach a constant value at $t \approx \lambda_{k1}$, which is generally lower than the time λ_{k2} required for $G(t,\gamma)$ to become truly factorable. The minimum in $h(\gamma,t)$ is observed at shear strains as low as 2.0 but becomes sharper as shear strain increases. This indicates that it is a feature of the materials nonlinear response. $h(\gamma,t)$ from over 20 different PS/DEP solutions also indicate that the size of the minimum is a function of polymer

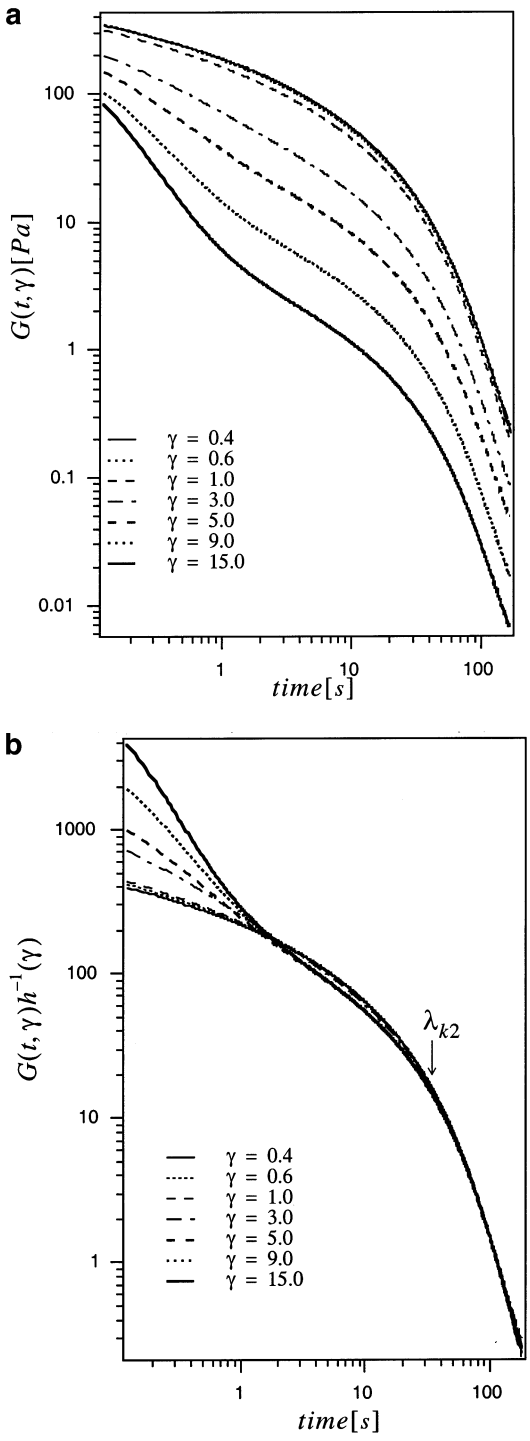

Figure 3. (a) Nonlinear shear relaxation modulus $G(t,\gamma)$ for PS8.4M6% at 28.5 °C. Measurements were performed using 50 mm diameter cone-and-plate fixtures roughened by attachment of a layer of 10−30 μm diameter glass beads. Shear strains γ ranging from 0.4 to 15.0 were used for these measurements. Strain increases from top to bottom in this figure. (b) Shifted nonlinear shear relaxation moduli $G(t,\gamma)$ $h(\gamma)^{-1}$ for PS8.4M6% at 28.5 °C. The arrow in the figure locates the time λ_{k2} beyond which nonlinear shear relaxation moduli $G(t,\gamma)$ can be factorized (approximately) into separate strain-dependent, $h(\gamma)$, and time-dependent, $G(t)$, functions.

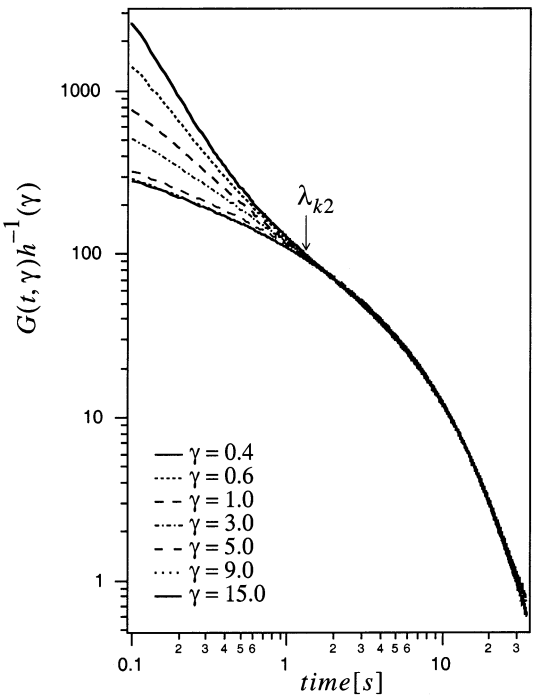

Figure 4. Shifted nonlinear shear relaxation moduli $G(t,\gamma)$ $h(\gamma)^{-1}$ for PS3.8M8% at 28.5 °C. Shear strains γ ranging from 0.4 to 15.0 were used for these measurements.The arrow in the figure locates the separability time λ_{k2}.

entanglement density. Specifically, for moderately entangled solutions, such as PS3.8M8%, the minimum is virtually nonexistent (see Figure 5b), while for more highly entangled materials such as PS20M6%, it is quite prominent (see ref 10). Furthermore, the presence of a local minimum in $h(\gamma,t)$ appears to coincide with the appearance of complicated transients in $G(t,\gamma)$ $h(\gamma)^{-1}$ discussed previously, and with separability times λ_{k2} that are equal to or larger than the terminal relaxation time τ_{d0}. The physical processes that produce the minimum are therefore very likely the source of delayed factorability in well-entangled PS/DEP solutions.

The fact that $h(\gamma,t)$ does not converge to a constant long-time value may be rigorously interpreted as evidence for weak nonfactorable behavior. A perhaps obvious concern is whether this behavior arises from measurement artifacts such as wall slip. To address this concern, Figure 5a presents $h(\gamma,t)$ data for the lowest ($\alpha = 1°$: open symbols) and highest ($\alpha = 5°$: filled symbols) cone angles. As discussed earlier, the shearing surfaces of both cone and plate were roughened using grafted beads to reduce wall slip errors. Although small differences in $h(\gamma,t)$ are evident, very little change in the size of the minimum is observed for a nearly 5-fold increase in the gap, indicating that errors due to interfacial slip cannot account for the behavior observed.

Relationships between λ_{k1}, λ_{k2}, and τ_{d0} for the PS/DEP solutions investigated in this and the previous study[10] are explored in Figure 6. The effect of polymer volume fraction and molecular weight, $\phi\bar{M}_w$, on separability and terminal times are also summarized in this figure. It is evident from the figure that for the entire set of materials studied, λ_{k2} is rather strongly aligned with τ_{d0} for solutions with $\phi\bar{M}_w > 5 \times 10^5$ g/mol. In fact, even the effect of $\phi\bar{M}_w$ on λ_{k2}, $\lambda_{k2} \sim (\phi\bar{M}_w)^3$, is consistent with expectations for τ_{d0}.[11] On the other hand, the observed scaling $\lambda_{k1} \sim (\phi\bar{M}_w)^{1.5}$ is not too different from the expected result for a relaxation process dominated by Rouse retraction with a contribution from a concentration-dependent monomeric friction coefficient. It is also apparent from Figure 6 that, for materials with $\phi\bar{M}_w \leq 5 \times 10^5$ g/mol and ($N/N_e(\phi) \leq 8$), λ_{k1} and λ_{k2} are similar in magnitude. On the basis of these results, it can be

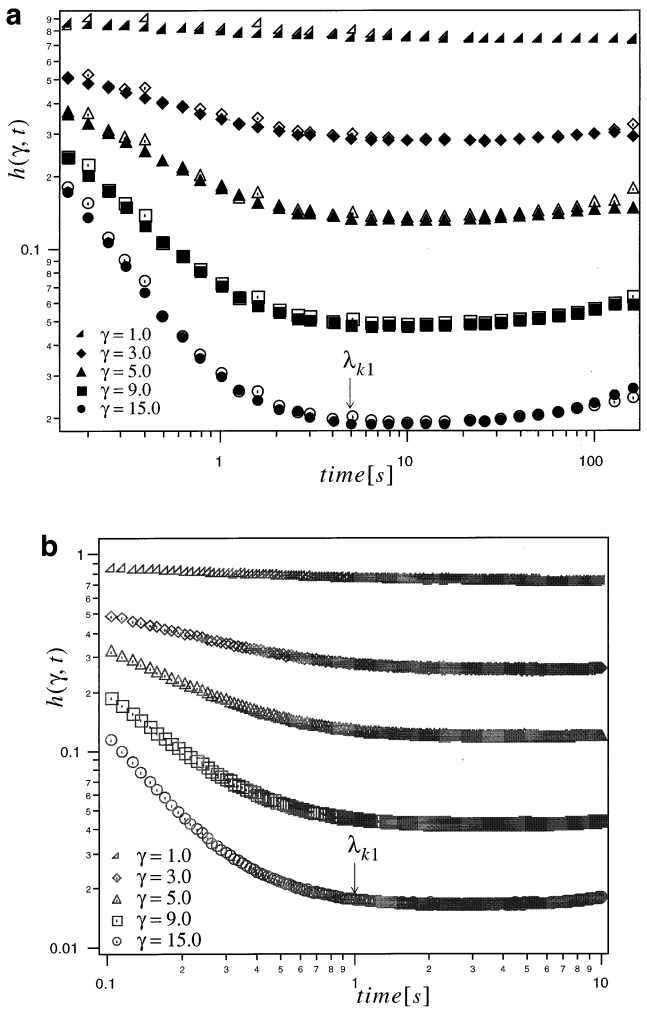

Figure 5. (a) Apparent step shear damping function $h(\gamma,t)$ for PS8.4M6% at 28.5 °C. The arrow locates the time λ_{k1} at which $h(\gamma,t)$ appears to become independent of time (i.e., when $h(\gamma,t)$ is plotted on a linear scale). (b) Same as for (a), but for PS3.8M8%.

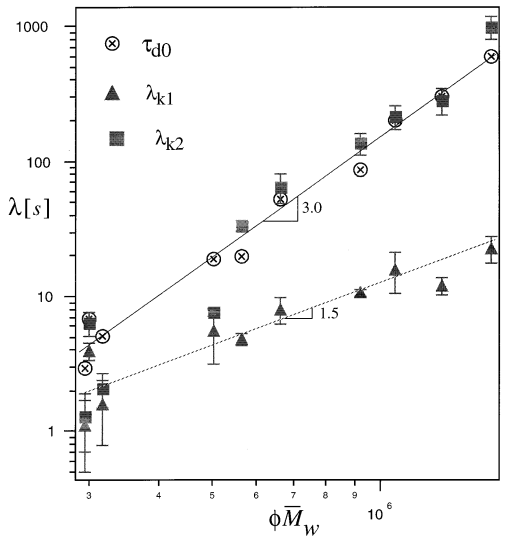

Figure 6. Effect of PS volume fraction ϕ and molecular weight M_w, $\phi\bar{M}_w$, on the terminal time τ_{d0}, separability time λ_{k2}, and apparent separability time λ_{k1} of PS/DEP solutions. Data in the figure are for solutions used in this and the previous part of the study.[10] The best-fit straight lines through the data support the following relations: $\tau_{d0} \sim \lambda_{k2} \sim (\phi\bar{M}_w)^3$ and $\lambda_{k1} \sim (\phi\bar{M}_w)^{1.5}$.

concluded that a Rouse mechanism for polymer chain stretch relaxation and/or tube reorganization is consistent with experimental observations only for moderately entangled PS/DEP solutions. In more entangled solutions, a second process becomes important. Molecular scale physics that can produce this process are discussed further in section 3.2.

Figure 7a presents short-time ($t \approx 0.25$ s) and long-time ($t \geq \lambda_{k2}$) step shear damping functions $h(\gamma)$ for PS8.4M6% measured using cone-and-plate fixtures with a wide range of cone angles α. The continuous line in the figure is the prediction h_{DE-IA} provided by the Doi–Edwards theory, with the independent alignment approximation. Broken lines are the short-time and long-time damping functions predicted using the analysis developed in section 3.2. Considering the extremely good correspondence of $h(\gamma)$ over the range of cone angles studied, interfacial slip errors are again seen to be insignificant in these experiments. It is also clear that the damping function at long times is well described by both theories, except perhaps at low shear strains where small negative deviations are apparent. The short-time damping function agrees quite well with predictions provided by the theory in section 3.2. Similar results were observed for all polymers used in the study. Data for PS3.8M8% are, for example, provided in Figure 7b. The open symbols represent the long-time damping function, while the closed symbols are the results for $t = 0.1$ s $\approx 0.5\tau_{Rouse}$, which is about 3−4 times the time required to achieve the target step strain for this material. Again the long-time data are in good accord with h_{DE-IA} as well as with predictions provided by eqs 2 and 5 (see section 3b). The short-time damping function predicted by eqs 2 and 5 is also seen to be in excellent accord with the experimental observation over the range of shear strains studied.

3.2. Theory. Mhetar and Archer proposed a mechanism for chain stretching and entanglement relaxation dynamics that accommodates processes other than the usual Rouse retraction dynamics.[4] In this section we will formulate a simple, closed-form equation for stress relaxation in entangled polymers that includes such processes. As in previous work, our objective here is not constitutive equation development, but rather to determine what physics is needed to reproduce salient features of polymer dynamics seen experimentally. Specifically, we wish to determine whether the transition from Rouse stretch relaxation in moderately entangled solutions to coupled stretch and orientation relaxation dynamics in more entangled materials can be explained in terms of the partial retraction and disentanglement/reentanglement processes envisaged by Mhetar and Archer.[4]

Our starting point is the tube model expression for stress on time scale $t > \tau_e$

$$\sigma_{ij} = c\langle F_T L_T u_i u_j\rangle \approx 3kT_c(L_T/D_B)\langle u_i u_j\rangle^{2,16} \qquad (1)$$

where τ_e is the Rouse relaxation time of polymer segments between entanglement points, c is the number density of chain segments, L_T is the occupied tube length, $D_B = \sqrt{N_e}b$ is the blob or equilibrated tube diameter, and $\langle u_i u_j\rangle = S_{ij}$ is the second moment tensor of polymer segment orientation vectors. We will use a differential equation proposed by Archer and Mhetar

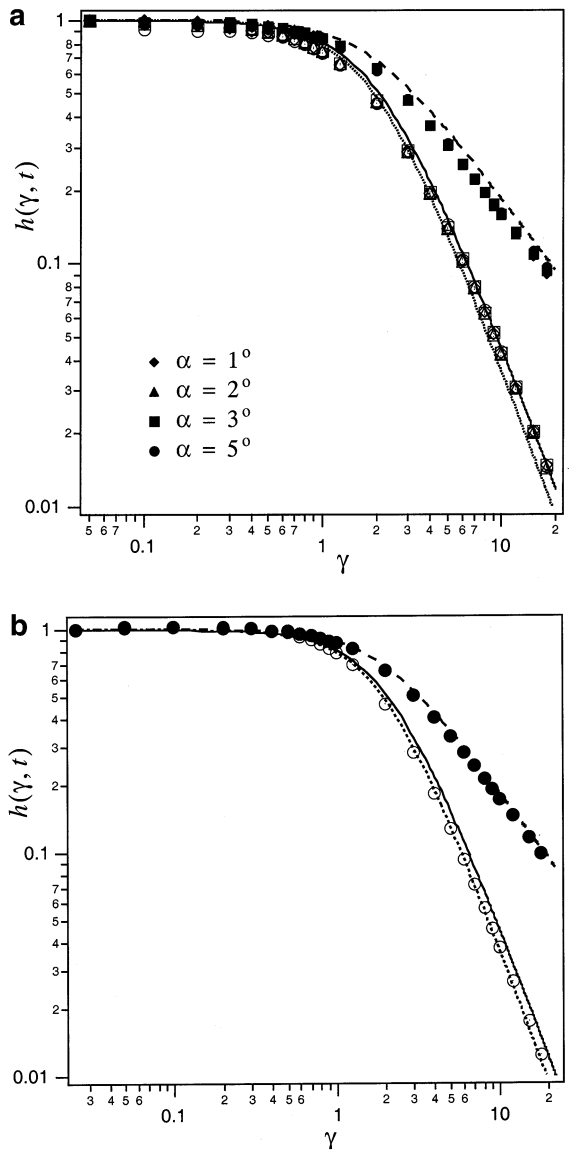

Figure 7. (a) Long-time ($t > \lambda_{k2}$) and short-time ($t = 0.25$ s) shear damping function $h(\gamma)$ for PS8.4M6% measured using cone-and-plate fixtures with four different gap angles α. All shear fixtures were roughened using 10−30 μm glass beads to minimize wall slip. Continuous line through the data is the damping function predicted by the Doi−Edwards theory with the independent alignment approximation.[2] The broken line is the short-time ($t \approx \tau_{\text{Rouse}}$) prediction of eqs 2 and 5 (see section 3.2). Dots represent the damping function $h(\gamma) = (1 + {}^{4}/_{15}\gamma^2)^{-1}$ predicted of eqs 2 and 5 at times $t \geq \lambda_{k2;\text{T}}$. (b) Same as (a), except data are for PS3.8M8%, and the results are for a single cone angle $\alpha = 5°$.

to describe the evolution of S_{ij} in shear flow[17]

$$\frac{\partial S_{ij}}{\partial t} + \frac{1}{\tau_{\text{d0}}}(S_{ij} - S_{ij,0}) - S_{im}\kappa_{mj} - \kappa_{in}S_{nj} + \frac{1}{3}(S_{ij}S_{mn} + S_{im}S_{nj} + S_{in}S_{mj})D_{mn} = 0 \quad (2)$$

Here κ is the velocity gradient tensor, and D is the symmetric part of the velocity gradient tensor. $\tau_{\text{d0}} \approx \tau_m N^2(N/N_{\text{e}})^{1+x}$ is the orientation relaxation time, where $x \approx 0.5$. Predictions of eq 2 for polymer rheology in various shear and extensional flows have been studied in some detail in ref 17. These predictions are generally intermediate between those obtained using the exact Doi−Edwards integral constitutive equation and the Doi−Edwards equation with the independent alignment approximation.[17] If L_{T} and D_{B} are taken to be constants, the solution of eqs 1 and 2 for the shear stress in a step shear deformation is

$$\sigma_{xy}(\gamma,t) = \gamma G(\gamma,t) = \frac{\gamma}{1 + (4/15)\gamma^2}\frac{15}{4}G_N \exp[-t/\tau_{\text{d0}}] \quad (3)$$

The step shear damping function follows from eq 3:

$$h(\gamma) = \frac{1}{1 + (4/15)\gamma^2} \quad (4)$$

Generally, neither L_{T} nor D_{B} is constant during stress relaxation following step shear. In an earlier article it was in fact shown that the evolution of $L_{\text{T}}/D_{\text{B}}$ can be described in terms of an evolution equation for the entanglement density per chain:[16]

$$L_{\text{T}}/D_{\text{B}} = (N/N_{\text{e0}})(1 + [\lambda - \lambda^{-1/2}]\exp\{-\tau/\tau_{\text{Rouse}}\} + [\lambda^{-1/2} - 1]\exp\{-t/\tau_{\text{CR}}\}) \quad (5)$$

Here, N_{e0} is the entanglement spacing at equilibrium, λ is the effective deformation experienced by tube segments, and $\tau_{\text{CR}} = AN^2(N/\tilde{N}_{\text{e}})^{2+x}\tau_m$ is the constraint release or tube renewal time.[19,18] A is a constant of order ${}^{2}/_{9}$,[18] x is of the order 0.5,[19] τ_m is the segmental relaxation time, and $N/\tilde{N}_{\text{e}}$ is the average entanglement density of polymer chains following retraction.

The second term in eq 5 accounts for entanglement loss during Rouse retraction. This term also captures the fact that the equilibrium contour length of an affinely deformed test molecule is not completely restored by Rouse retraction.[4] The last term in eq 5 describes the restoration of entanglements following retraction. Although the process by which polymer chains reentangle is presently unknown, a fair estimate of the time required for a molecule to fully recover its equilibrium entanglement density is τ_{CR}, the tube renewal time. Because $N/\tilde{N}_{\text{e}}$ decreases with increasing strain,[4] the initial reentanglement rate is faster at high shear strains. $N/\tilde{N}_{\text{e}}$ increases with time as chain entanglements are restored, so the reentanglement rate decreases with time at all shear strains. To produce a closed formula for $L_{\text{T}}/D_{\text{B}}$ that captures these two effects, we here approximate $\tilde{N}_{\text{e}}$ using the postretraction expression for polymer entanglement spacing derived elsewhere.[4] Substituting for $\tilde{N}_{\text{e}}$ in the formula for τ_{CR} and rearranging yields

$$\tau_{\text{CR}} \approx \frac{2}{9}N^2\left(\frac{N}{N_{\text{e0}}}\right)^{2+0.5}\lambda^{1.25}\tau_m \approx \frac{2}{9}\left(\frac{N}{N_{\text{e0}}}\right)\lambda^{1.25}\tau_{\text{d0}} \quad (6)$$

with $\lambda = [1 + (4/15)\gamma^2]^{1/2}$. Equation 6 can now be inserted into eq 5 to provide our final evolution formula for $L_{\text{T}}/D_{\text{B}}$. This equation can be solved along with eq 2 and the results substituted in eq 1 to yield any component of the polymer stress tensor following nonlinear step shear.

Figure 8a,b summarizes $G(t,\gamma)$ and $G(t,\gamma)\ h(\gamma)^{-1}$ predictions of eqs 2 and 5 for PS8.4M6% (i.e., using $N/N_{\text{e0}} = 13$, $\tau_{\text{d0}} = 2.41$ s, $\tau_{\text{Rouse}} = 0.49$ s, and $G_{\text{N}} = 375$ Pa), for the same set of shear strains in Figure 3a,b. The corresponding short-time and long-time damping functions predicted by the theory have already been

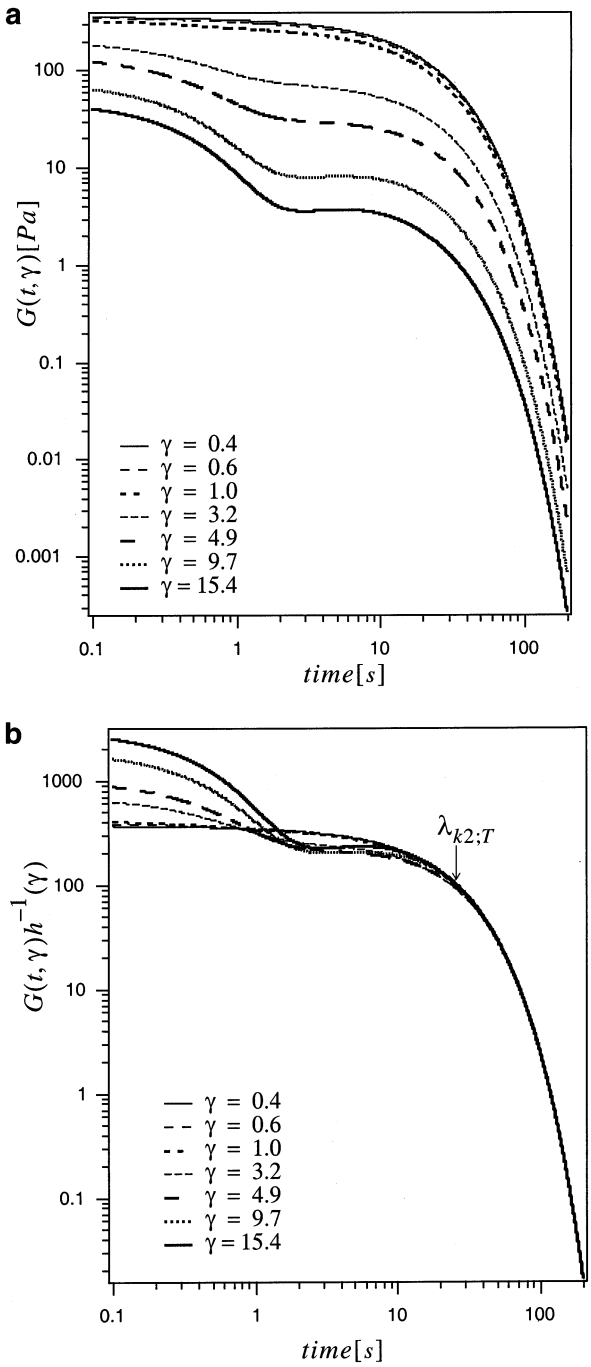

Figure 8. (a) $G(t,\gamma)$ predicted by eqs 2 and 5 for PS8.4M6%. Strain increases from top to bottom in the figure. (b) $G(t,\gamma)\ h(\gamma)^{-1}$ predicted by eqs 2 and 5 for PS8.4M6%. The arrow locates the theoretical separability time $\lambda_{k2;T}$.

compared with experimental data in Figure 7a. Some features of the experimental results are clearly missing from the theoretical predictions. The theoretical $G(t,\gamma)$, for example, suggests that very little relaxation occurs between τ_{d0} and τ_{Rouse}, but the equivalent experimental results (Figure 3a) manifest quite a bit of relaxation on intermediate time scales. This difference can be narrowed by considering a spectrum of relaxation events in the analysis. The curvatures of the experimental and theoretical $G(t,\gamma)\ h(\gamma)^{-1}$ data at high strains and early times are also clearly different. We suspect that this discrepancy also arises from omission of contributions from faster Rouse and/or contour length fluctuation modes to the material's relaxation spectrum.

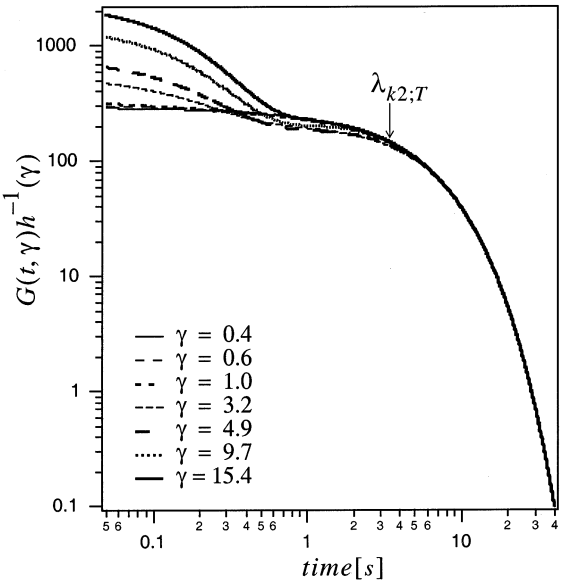

Figure 9. $G(t,\gamma)\ h(\gamma)^{-1}$ predicted by eqs 2 and 5 for PS3.8M8%. The arrow locates the theoretical separability time $\lambda_{k2;T}$.

Many features of the experimental results are nonetheless captured quite well by the analysis. For example, the inflection in $G(t,\gamma)$ at $t \approx 2\tau_{Rouse}$ is observed in both the experimental and theoretical plots. The complicated transients in $G(t,\gamma)\ h(\gamma)^{-1}$ seen in the experimental data prior to time strain factorability is also reproduced by the theory. The separability time is correctly predicted to be substantially larger than τ_{Rouse}. Furthermore, the average τ_{k2} values determined from experiment and from the theoretical predictions are of the correct magnitude (see Table 2). Finally, the theoretical and experimental step shear damping functions at short times ($t = 0.5\tau_{Rouse}$) as well as at long times ($t \geq \tau_{k2}$) following imposition of step shear are in good to excellent accord (see Figure 7a). Thus, eqs 2 and 5 capture most features of the step shear response of PS8.4M6%.

$G(t,\gamma)\ h(\gamma)^{-1}$ predictions for PS3.8M8% are provided in Figure 9 for the same range of shear strains studied experimentally (see Figure 4). It is immediately apparent from the plot that the short-time complex crossing of $G(t,\gamma)\ h(\gamma)^{-1}$ curves at high and low shear strains observed for PS8.4M6% are noticeably reduced, in agreement with the experimental results. The crossing behavior is predicted to completely disappear for materials with $N/N_{e0} \leq 4$, which is lower than observed experimentally. However, this prediction depends on the values of A and x used in τ_{CR}. These values are currently not known with sufficient precision to rule out a moderately higher threshold for onset of the complex short-time $G(t,\gamma)\ h(\gamma)^{-1}$ behavior. The theoretical separability time $\lambda_{k2} = 16\tau_{Rouse}$ is larger than observed experimentally, but the ratio $\lambda_{k2}/\tau_{Rouse}$ is noticeably smaller than for PS8.4M6%, which is also consistent with observations from experiments. Experimental and theoretical damping functions for PS3.8M8% are compared in Figure 7b. Again, both the short-time and long-time damping behavior observed experimentally are clearly captured by this theory.

Perhaps the most unusual observation in the response of entangled PS/DEP solutions to large-amplitude step strain is that the apparent shear damping function $h(\gamma,t)$ displays a shallow local minimum at a time of order 5−15 times τ_{Rouse}. This behavior cannot be reproduced using molecular constitutive theories that only

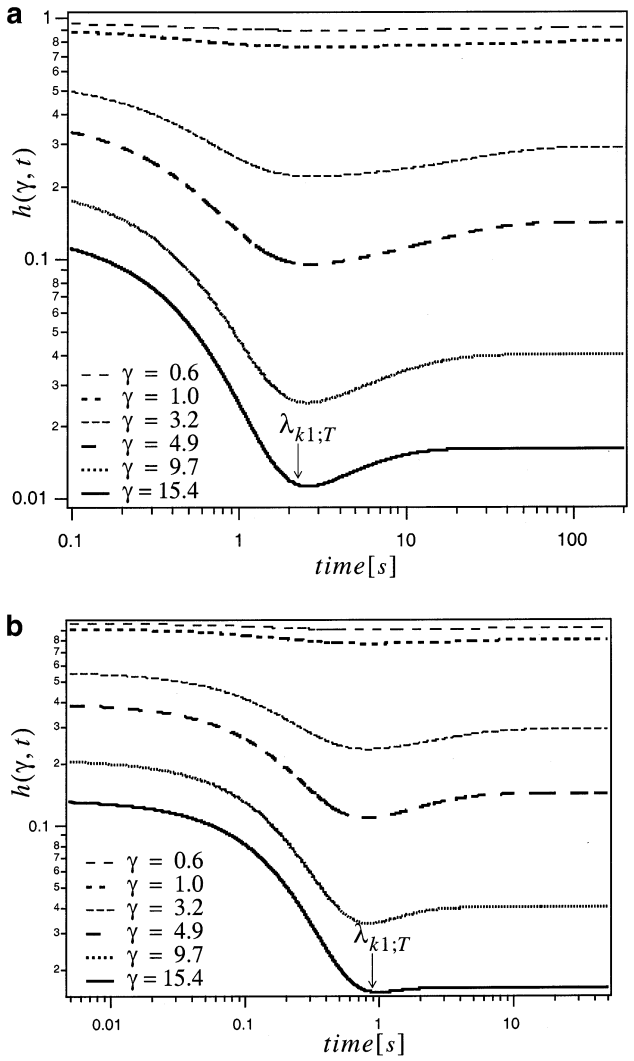

Figure 10. (a) Apparent step shear damping function $h(\gamma,t)$ for PS8.4M6% predicted by eqs 2 and 5. The arrow locates the apparent separability time $\lambda_{k1;T}$. (b) Same as for (a), but for PS3.8M8%.

account for stretch and orientation relaxation processes following step shear, because the minimum implies stress growth with time. A mechanism wherein entangled polymers respond to step strain by initially losing entanglements with their neighbors and then slowly regaining these entanglements can in principle explain the observed behavior. Such a mechanism is captured by eq 5. Theoretical predictions of $h(\gamma,t)$ for PS8.4M6% and PS3.8M8% are provided in Figure 10a,b. It is evident from these plots that the theory correctly captures the minimum for PS8.4M6%, as well as the near absence of one for PS3.8M8%. The apparent separability time $\lambda_{k1;T}$, i.e., the time at which $h(\gamma,t)$ appears to become constant on a linear scale, is also correctly predicted to be of order $5\tau_{\text{Rouse}}$ for both materials (see Table 2). Similar $h(\gamma,t)$ features are predicted for the other two polymers studied; $\lambda_{k1;T}$ values for these materials are also provided in Table 2. Considering the uncertainty in determining λ_{k1}, the agreement between theoretical predictions and experimental results is quite good. The shapes of the theoretical $h(\gamma,t)$ minima are nonetheless somewhat different from the experimental observations. Specifically, the theoretical minima are narrower and better defined that those seen experimentally. This discrepancy can be traced to uncertainty in the values of A and x used in the analysis and to the narrowness of the relaxation spectrum considered in the theory.

4. Conclusions

Stress relaxation dynamics of entangled solutions of high molar mass polystyrenes in diethyl phthalate were investigated in nonlinear step shear flows using mechanical rheometry experiments and theory. Experiments were performed using several large-diameter (50 mm) cone-and-plate measurement fixtures, cone angles α in the range $1° \leq \alpha \leq 5°$, that were roughened by attachment of a single layer of 10−30 μm silica glass beads to the cone-and-plate surfaces. These fixtures facilitate measurements of nonlinear shear relaxation moduli $G(t,\gamma) \equiv \sigma_{xy}(\gamma,t)/\gamma$ that are uncorrupted by wall slip errors. $G(t,\gamma)$ data obtained using these procedures are of unprecedented accuracy, particularly at long times. A simple theory for stress relaxation dynamics in entangled polymers that accounts for coupled relaxation of molecular orientation, chain stretching, and polymer entanglement density in step shear was also developed and used to analyze experimental results.

The main findings of the study can be summarized as follows: (i) In entangled polymers $G(t,\gamma)$ can be factorized into separate strain-dependent and time-dependent functions only after a time λ_{k2} substantially larger than the longest Rouse relaxation time τ_{Rouse} of the solution. For polymer solutions with $\phi\bar{M}_w \geq 5 \times 10^5$ and $N/N_e(\phi) \geq 8$, λ_{k2} varies with polymer volume fraction ϕ and molecular weight $\bar{M}_w$ in the same manner as the terminal or disengagement time τ_{d0}, $\lambda_{k2} \approx \tau_{d0} \sim (\phi\bar{M}_w)^3$. These findings are consistent with results reported in previous studies[8,10] but disagree with predictions of most current molecular theories for entangled polymers. We find, however, that a theory for stress relaxation based on partial recovery of polymer contour length on time scales of order τ_{Rouse}, followed by slower coupled entanglement and tube stretch relaxation processes on time scales of order the constraint release relaxation time, correctly reproduces the experimental observation. (ii) For PS/DEP solutions with $\phi\bar{M}_w < 5 \times 10^5$ and $N/N_e(\phi) \leq 6$, separability is observed after a time λ_{k1} of order 5−10 times τ_{Rouse}. The effects of polymer volume fraction ϕ and molecular weight $\bar{M}_w$ on the separability time, $\lambda_{k1} \sim (\phi\bar{M}_w)^{3/2}$, are also in fair accord with expectations for factorability based on a Rouse stretch relaxation mechanism. The transition from simple Rouse stretch relaxation processes to the more complex two-step chain stretch/entanglement relaxation mechanism described in (i) is also consistent with expectations from the theory for stress relaxation described in the article. (iii) The apparent shear damping function $h(\gamma,t)$ in well-entangled polymers displays an unusual local minimum at times of order λ_{k1}. As the entanglement density increases above eight, this feature becomes more noticeable and appears to be the origin of the much longer separability times in PS/DEP solutions with $\phi\bar{M}_w \geq 5 \times 10^5$. A local minimum in $h(\gamma,t)$ following step strain requires a mechanism of stress growth during relaxation. This behavior therefore cannot be explained by molecular theories that only account for polymer chain stretching and orientation relaxation processes following nonlinear step strain. A theory based on the idea that during retraction polymer chains lose entanglements, which are regained by slow reentanglement processes on time scales of order the tube reconstruction or

constraint release time, predicts $h(\gamma,t)$ features similar to those observed experimentally. We therefore conclude that polymer disentanglement/reentanglement dynamics in nonlinear step shear is the source of delayed factorability in well-entangled polymer solutions.

Acknowledgment. This study was supported by the National Science Foundation, Grant CTS0100579. We are grateful to Glen Swan of the Chemical Engineering machining shop for his assistance with the rheometer fixture designs used in the study. Scanned probe microscopy and dynamic contact angle measurement facilities at Cornell Center for Materials Research, funded through the National Science Foundation Division of Materials Research, were used for characterizing surface properties of the rheometer fixtures used in the study.

References and Notes

(1) de Gennes, P. G. *J. Chem. Phys.* **1971**, *55*, 572.
(2) Doi, M.; Edwards, S. F. *The Theory of Polymer Dynamics*; Oxford University Press: Oxford, 1986.
(3) Pearson, D. S.; Kiss, A. D.; Fetters, L. J. *J. Rheol.* **1989**, *33*, 517.
(4) Mhetar, V. R.; Archer, L. A. *J. Non-Newtonian Fluid Mech.* **1999**, *81*, 71.
(5) Einaga, Y.; Osaki, K.; Kurata, M.; Kimura, S.; Tamura, M. *Polym. J.* **1971**, *2*, 550.
(6) Fukuda, M.; Osaki, K.; Kurata, M. *J. Polym. Sci., Polym. Phys. Ed.* **1975**, *13*, 1563.
(7) Osaki, K.; Nishizawa, K.; Kurata, M. *Macromolecules* **1982**, *15*, 1068.
(8) Archer, L. A. *J. Rheol.* **1999**, *43*, 1555.
(9) Mhetar, V. R.; Archer, L. A. *Macromolecules* **1998**, *31*, 6639.
(10) Sanchez-Reyes, J.; Archer, L. A. *Macromolecules* **2002**, *35*, 5194.
(11) Ferry, J. D. *Viscoelastic Properties of Polymers*, 3rd ed.; Wiley: New York, 1980.
(12) Osaki, K.; Inoue, T.; Uematsu, T.; Yamashita, Y. *J. Polym. Sci., Part B: Polym. Phys.* **2001**, *39*, 1704.
(13) Menezes, E. V.; Graessley, W. W. *J. Polym. Sci., Polym. Phys. Ed.* **1982**, *20*, 1817.
(14) Inoue, T.; Yamashita, Y.; Osaki, K. *Macromolecules* **2002**, *35*, 1770.
(15) Inoue, T.; Uematsu, T.; Yamashita, Y.; Osaki, K. *Macromolecules* **2002**, *35*, 4718.
(16) Islam, M. T.; Sanchez-Reyes, J.; Archer, L. A. *J. Rheol.* **2001**, *45*, 61.
(17) Archer, L. A.; Mhetar, V. R. *Rheol. Acta* **1998**, *37*, 170.
(18) Lee, J. H.; Archer, L. A. *J. Polym. Sci., Part B: Polym. Phys.* **2001**, *39*, 2501.
(19) Monfort, J. P.; Marin, G.; Monge, P. *Macromolecules* **1984**, *17*, 1551.

MA021286Q